ISSN: 2710-2165

Synchronising the Hydraulics Model Builder and NDWI Indexes in Remote Sensing Techniques to estimate accurate Flood Hazard from Satellite Images

Khanssaa M. Abdul Majed[1], Shahad Mahgoob Nafl [2], Karam J. mohammed[3], Hanif Baharin[4], Puteri N.E. Nohuddin[5]

[1]Space Centre Technology, Scientific Research Commission, Baghdad, Iraq
Email: khanssaa.m.abdulmajed@src.edu.iq

[2]College of Medicine, University of Baghdad, Iraq
Email: shahad.m@comed.uobaghdad.edu.iq

[3]Space Centre Technology, Scientific Research Commission, Baghdad, Iraq
Email: karam.j.mohammed@src.edu.iq

[4]Institute of Visual Informatics, Universiti Kebangsaan Malaysia, Malaysia
Email: hbaharin@ukm.edu.my

[5]Higher Colleges of Technology, Sharjah, UAE
Email: pnohuddin@hct.ac.ae

Article History

Received: Jun. 09, 2026

Revised: Aug. 15, 2026

Accepted: Aug. 17, 2026

Abstract

Water resources are an important natural resource that sustains life and supports the growth of society and an economy. However, it remains an unusual resource that is not always available at the same time or in the same place. Climate change and global warming have worsened extreme weather events, such as heavy rain and flooding, in many parts of the world over the last few decades. This study aims to identify and map regions in Al-Shirqat at risk of flooding through analysis of Landsat 8 OLI data. A Hydraulics Model (HDM) was a distinct structural modelling tool within the ArcGIS environment that utilised the Python programming language to compute water depths from Digital Elevation Model (DEM) data. This suggested method improves standard analytical methods, which involve analysing images for the Normalised Difference Water Index (NDWI). This study's findings offer a pragmatic approach for enhancing flood risk evaluation and water resource management in analogous geographical contexts.

Keywords- Al-Shirqat region, Water resources, Flood hazard, Landsat 8 OLI, (HDM).

I. INTRODUCTION

Flood disasters are considered hydrological phenomena that arise from the accumulation or rise of water to the extent that it inundates the land, whether due to heavy rainfall or rising water levels in watercourses. It will lead to water exceeding its natural boundaries, resulting in floods that cause significant damage to lives and property. Due to the difficulty of controlling them, the most prominent of these are the damage caused by transportation, industrial and agricultural buildings and installations, livestock, utilities, and population, in addition to many economic difficulties [1], [2]. In this study, the areas affected by flooding in the Al-Sherqat area were observed using Landsat 8 OLI satellite imagery.

A. Problem Statement:

Flood hazard estimation relies heavily on accurate detection of surface water; however, this problem includes several specific challenges:

1) How can the underlying causes of flooding in a specific area be identified?
2) Which types of satellite imagery are most suitable for analysing flood-affected regions?
3) How can water levels, terrain slopes, and related measurements be accurately determined?
4) What methods and analytical approaches can be applied to study this problem?
5) What are the expected benefits and outcomes of applying these methods in flood analysis?

B. Objective of the Study:

This study aims to:

1) Identify the causes of flooding in affected areas using Landsat 8 OLI satellite imagery at 30-meter resolution to provide a clear understanding of the environmental and geographical factors contributing to flooding.
2) Determine water levels and topography slopes, and perform accurate measurements to assess flow velocity and calculate water discharge for each flood event. This analysis will help identify flood causes, support the implementation of effective water storage and management strategies, and understand the topographical characteristics of this area suitable for water retention.

C. Literature Review:

These are summaries of previous studies on river flow and flood calculations, as follows:

1) The first study (Riki & Utriweni, 2024) uses Geographic Information System (GIS) attributes to represent both graphic and non-graphic data. These data are stored in digital formats, including vector and raster data, which are associated with hard map elements and geographic locations, to improve the ability of integrated spatial analysis [3].
2) The second study (Purwadi et al., 2025) emphasises the use of Hyperspectral Image (HIS) in remote sensing classification, offering a wealth of information. In contrast, Hyperspectral Imaging (HSI) records intricate land-cover data across numerous narrow, contiguous wavelengths. These methods are difficult to use on large datasets because they require substantial computational power. Principal Component Analysis (PCA) is widely employed for HSI dimension reduction; yet, it frequently fails to capture local HSI characteristics that are essential for precise classification using global data [4].
3) The third study (Razi *et al*., 2024), which employed the Normalised Difference Water Index (NDWI) and the Modified Normalised Difference Water Index (MNDWI) algorithms, demonstrated that these algorithms are efficient tools for measuring water content and assessing liquefaction vulnerability in satellite images using Landsat 8 OLI imagery. Both indices were implemented through the Google Earth Engine (GEE) cloud-computing platform to enable precise spatial and temporal data processing [5].

II. THE STUDY AREA

A. Location Study Area:

The study area is located between the following geographical coordinates: **(**35°31′40″ to 35°29′10″ N) and (43°13′20″ to 43°15′00″ E)**,** as shown in Figure 1. The area is surrounded by hills from several directions: to the south by the Khattouka Hills, to the west by a series of scenic hills, and to the north by the Garnaf Hills, as well as other scattered elevations[6]–[8]. The region lies in the foothills of the Makhoul Mountains, within a semi-mountainous zone, and is characterised by long, narrow, and asymmetrical mountain bends**.**

The area's soil is productive, well-drained, and suitable for a wide variety of crops, depending on rainfall and groundwater resources. Groundwater is available through springs and artesian wells. The region's elevation ranges from 300 to 600 m above sea level**,** which supports the growth of grasses and trees and enhances agricultural productivity [9]–[11].

Al-Sharqat became a province from the Salah Al-Din Region; before 1987, it was administratively part of Nineveh Province. Nineveh Province borders it to the north and west, Baiji District to the south, and Kirkuk and Erbil Region to the east. The city is built upon the remains of the ancient historical city of Ashur. Its municipal boundaries extend northward to the village of Huraia, eastward to the Tigris River, and southward to the village of Sabkha. Figure 1 illustrates the geographical location of the study area in Iraq.

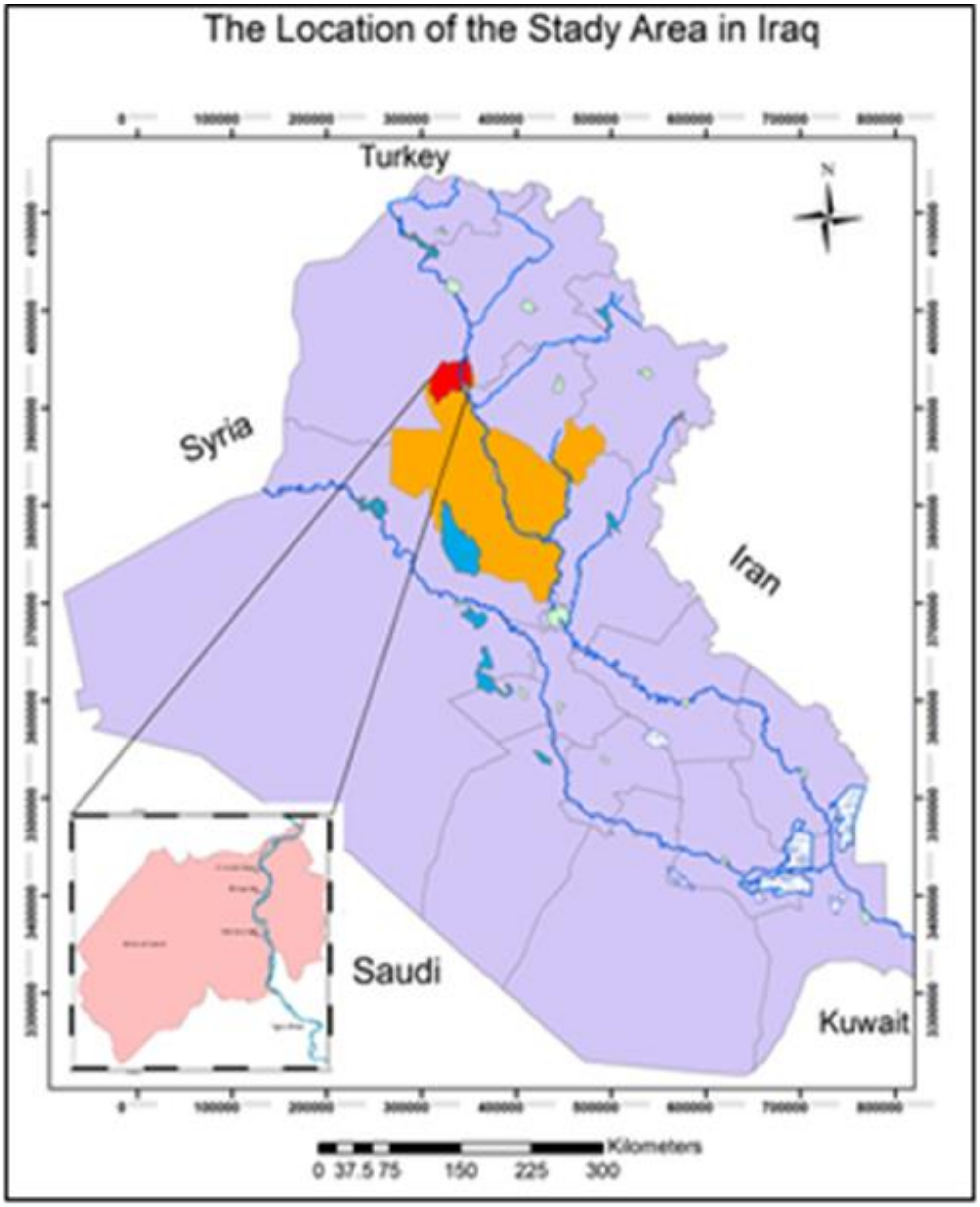

Fig. 1. The geographical location of the Al-Shirqat region in Salah Al-Din Governorate (researcher's work).

B. Climate of the Study Area:

The rain in Salah Al-Din Governorate is seasonal, accounting for about 90% of the annual rainfall between November and April. While the other six months are mostly dry and hot, as represented in June and August, this climate environment is characterised by low rainfall and hot temperatures. Therefore, due to these extreme climates, some parts of the governorate can be considered desert or semi-desert regions, where plants and soil lose moisture rapidly due to high evaporation rates. As a result, Salah Al-Din Governorate is one of the Iraqi provinces most affected by the significant weather disparities [7].

III. METHODOLOGY AND MATERIALS

A. Methodology:

The premise of this research is founded on the use of two methodologies, a conventional approach and a proposed way, to identify the regions impacted by flooding during the study duration. These methods rely on the analysis and processing of satellite images, as described below:

1) Normalised Difference Water Index (NDWI): NDWI is a spectral index derived from satellite image reflectance values. It is widely used to identify and describe surface water bodies by enhancing the water features while suppressing vegetation and soil reflectance.
2) Hydraulics Model: This method determines water flow directions and surface slopes within the study area using contour data**.** It enables the identification of flood-prone zones by modelling water movement across the terrain. The overall methodological framework of this research is illustrated in the following figure**.**
3)

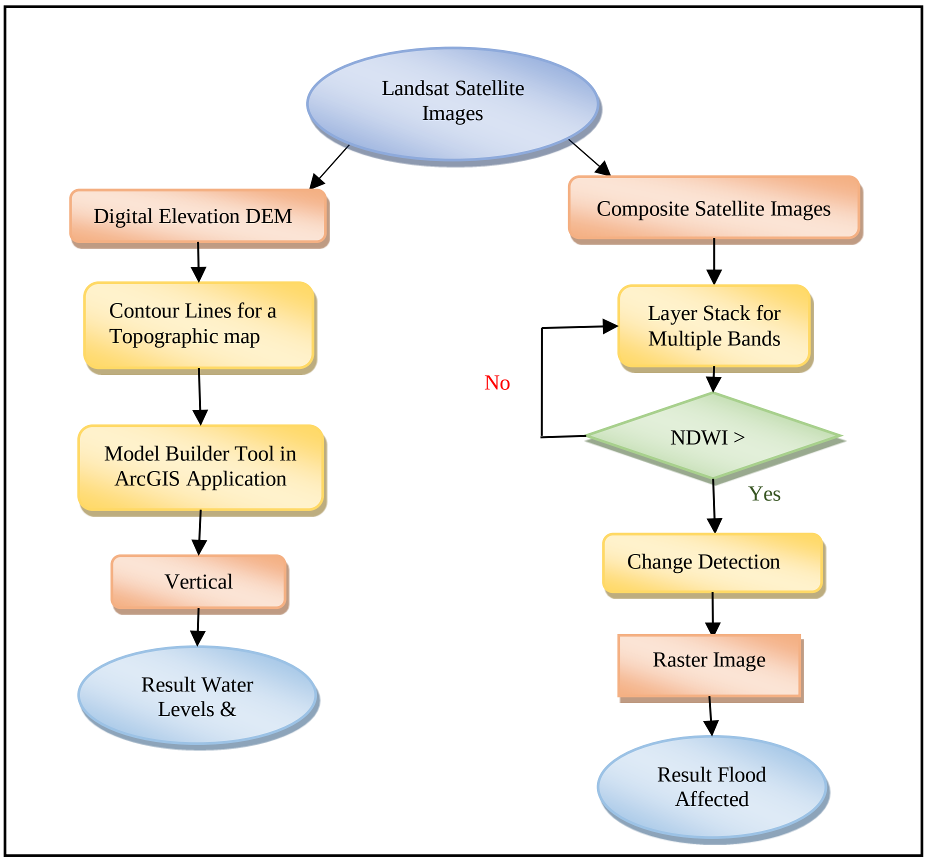

Fig. 2. The Structure methods of this research.

B. Data Used:

Remote sensing data are primary sources for analysing environmental processes at local and global scales. These data are used to detect changes over recent decades compared with older decades. Remote sensing data (such as Landsat and Sentinel data) are very useful for visualisation, classification, and analysis of the area.

In this paper, satellite images from the USGS Landsat 8 Collection 2 Tier 1 TOA Reflectance are used, which are available from USGS Earth Explorer. However, it used images of remotely sensed data such as; images of Landsat 8 in dates 11 November 2018 and 29 Des. 2018, for the study area, as shown in Figure 3, in addition used Lindsat8 satellite images in dates 2 Des. 2020 and 12 November 2023 as illustrated in Figure 4 to contrast the flood affected area with Geo-Processing and analysis steps by NDWI Index, change detection, and Model Builder Tool (MBT) to implement the Hydraulics model for the images by using ERDAS IMAGIN 2014, and ArcMap10.8 respectively.

C. Composite Satellite Images:

Landsat 8 data uses 12 bands, each covering the visible, near-infrared, and shortwave-infrared spectral regions. The various spatial resolutions for Landsat 8 bands have been confined between (15m/pixel – 30 m/pixel), which means for every meter per pixel [12]. The Landsat-8 data bands, wavelengths, and resolutions are given in Table I below.

TABLE I. LANDSAT 8 OLI DATA'S BANDS, WAVELENGTH & THEIR RESOLUTION (GOOGLE EARTH ENGINE).

Name	Description	Resolution	Wavelength
B1	Coastal aerosol	30 meters	0.43 - 0.45 µm
B2	Blue	30 meters	0.45 - 0.51 µm
B3	Green	30 meters	0.53 - 0.59 µm
B4	Red	30 meters	0.64 - 0.67 µm
B5	Near infrared	30 meters	0.85 - 0.88 µm
B6	Short-wave infrared 1	30 meters	1.57 - 1.65 µm
B7	Short-wave infrared 2	30 meters	2.11 - 2.29 µm
B8	Band 8 Panchromatic	15 meters	0.52 - 0.90 µm
B9	Cirrus	30 meters	1.36 - 1.38 µm
B10	Thermal infrared 1, resampled from 100m to 30m	30 meters	10.60 - 11.19 µm
B11	Thermal infrared 2, resampled from 100m to 30m	30 meters	11.50 - 12.51 µm
QA_PIXEL	Landsat Collection 2 OLI/TIRS QA Bitmask	30 meters	

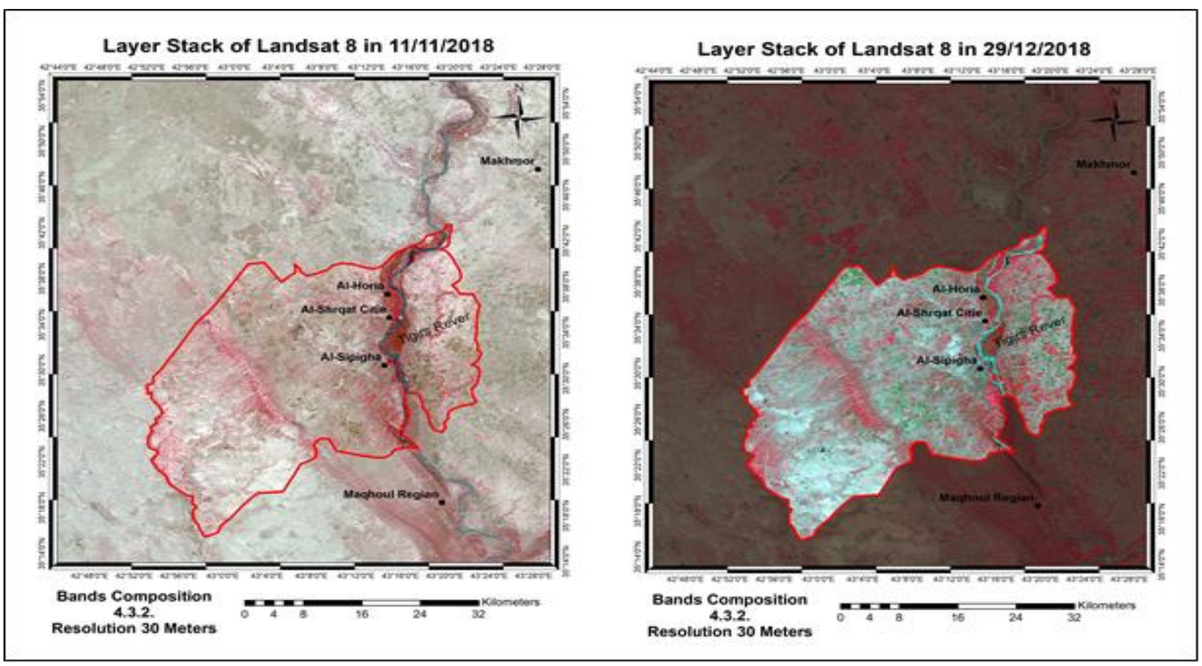

Fig. 3. Landsat 8 OLI Composition bands of the Al-Sharqat region in 11/11/2018, & 29/12/20118 (USGS)

This study, utilises satellite imagery from Landsat 8, which include visible bands, near infrared (NIR) band, Short-wave Infrared (SWIR1-2) bands for Operational Land Imager (OLI) for multispectral Landsat 8 bands in spectral spatial resolution (30m), for visible bands as illustrated in Figure 3, which depended on the Landsat-8 layer stack [14] from 11/11/2018 and 29/12/2018 represents a composite of multiple multispectral reflectance bands, and the layer stack of Figure 4 [13] on the 2/12/2020, with 17/11/2023 for the study area [12].

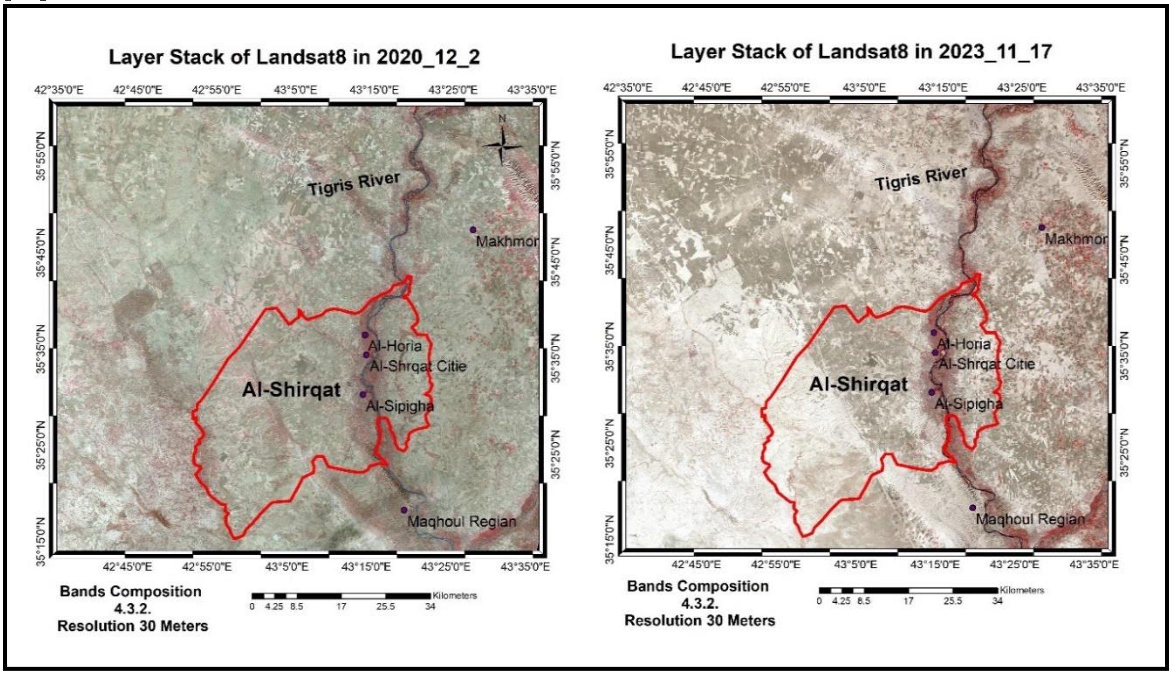

Fig. 4. Landsat8 Composition bands in 2/12/2020 & 17/11/2023 (USGS [14]).

IV. PROCESSING AND CLASSIFYING SATELLITE IMAGES

A. The Normalised Difference Water Index (NDWI):

This index is used to extract various water body types, including pure water, turbid water, salt water, and floating ice. In Landsat 8, the spatial resolutions of the NIR and Green bands are both equal resolution (30 m). Thus, in this research, the NDWI can be directly calculated using the 2 equations [6].

$$NDWI = (Green - NIR) / (Green + NIR) \quad (1)$$

$$Landsat\ 8\ NDWI\ Formula = (B3 - B5) / (B3 + B5) \quad (2)$$

The Normalised Difference Water Index (NDWI) is an index derived from the Green band (Band 3 of the Landsat 8 data) and denotes the reflectance of the green band. NIR denotes the reflectance of the near-infrared band (Band 5 of the Landsat 8 imagery). As a result, the following satellite images are shown in Figures 5 and 6.

Thus, with specific band numbers varying by sensor in this study, the satellite images were classified using Landsat 8 OLI imagery to apply the water index to determine water bodies, and the NDWI's water body detection capability was evaluated [15] as follows:

It is produced the closest result of the water body (0.13) deviations of spectral reflectance for both dates (11/ 11/ 2018) before the flooding event and (29/ 12/ 2018) after the overflow event, and the water body deviations of optical reflectivity between (0.10) to (0.12) for dates (2/ 12/ 2020 and 17/ 11/ 2023) respectively which represented the dry year with the rainy year compared to it, and the Table II is illustrated the result of the NDWI equations:

TABLE II. THE BANDS AND WAVELENGTHS AND THE RESULTS OF THE SPECTRAL REFLECTANCE OF THE NDWI EQUATIONS.

Bands Name	Resultion	Wavelength	Description	Dates	Spectral Reflectance of NDWI equations
B3 /Green	30 m	0.53 - 0.59 µm	Before overflow	11/11/2018	0.13µm
			After overflow	29/12/2018	0.13µm
B5 /NIR infrared	30 m	0.85 - 0.88 µm	Dry year	2/ 12/ 2020	0.10µm
			After flooding	17/11/2023	0.12µm

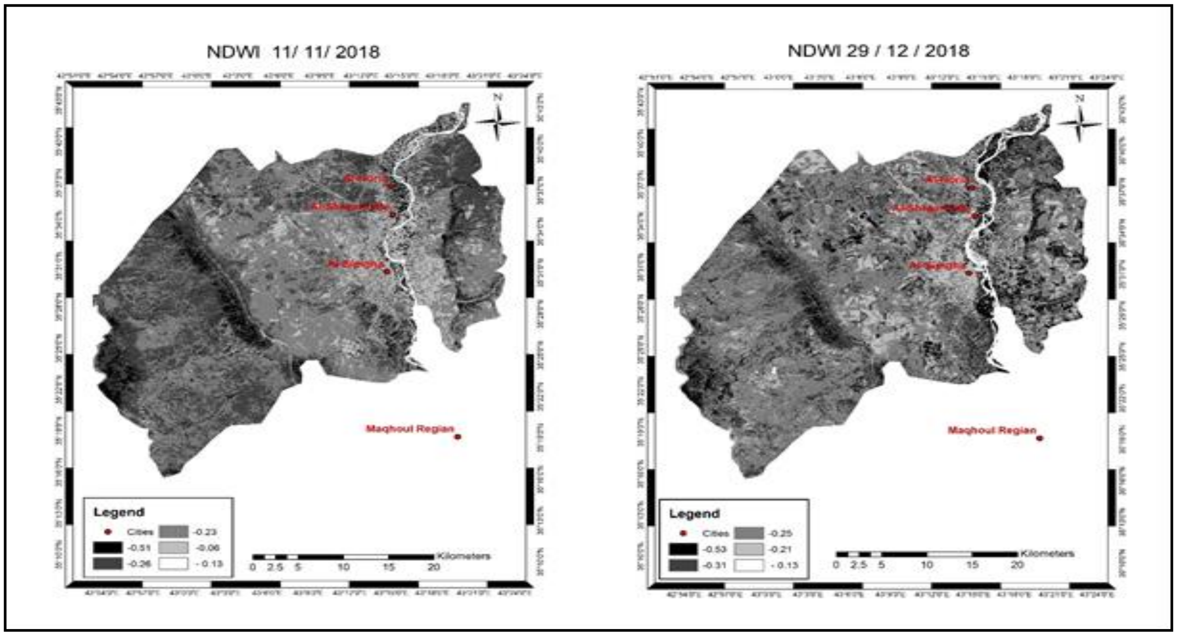

Fig. 5. Analyse satellite images using the (NDWI) formula result.

ISSN: 2710-2165

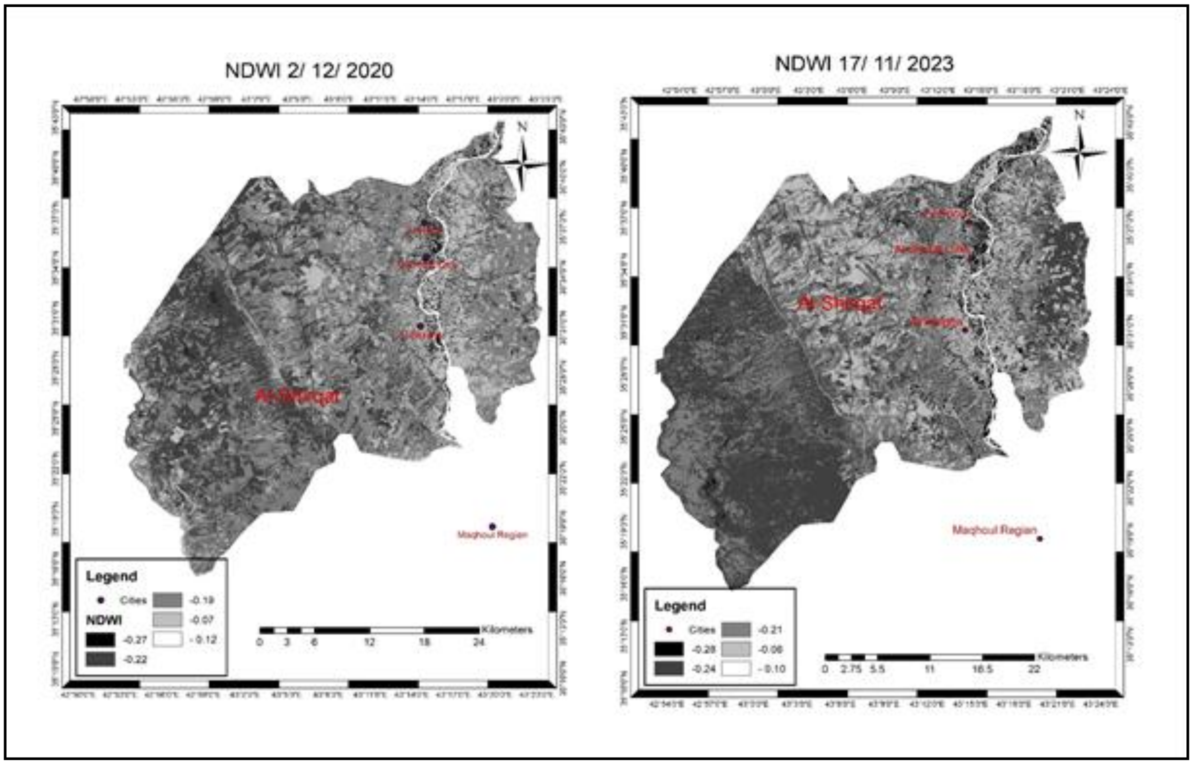

Fig. 6. Analysis of satellite images using the (NDWI) formula results.

B. Change Detection:

It is one of the most important modern technology systems in ERDAS applications for monitoring and detecting environmental changes [16], which can be used to study changes that occur in specific areas, such as forests, rivers, lakes, soil, and natural vegetation. Therefore, to detect a change in a specific area, we need two satellite images of equal accuracy, with the same size and pre-corrected using the water index, as illustrated in Figure 7. That showed an increase in green colour with a low rate of change, and a decrease in red colour in areas almost affected by flood waters [9].

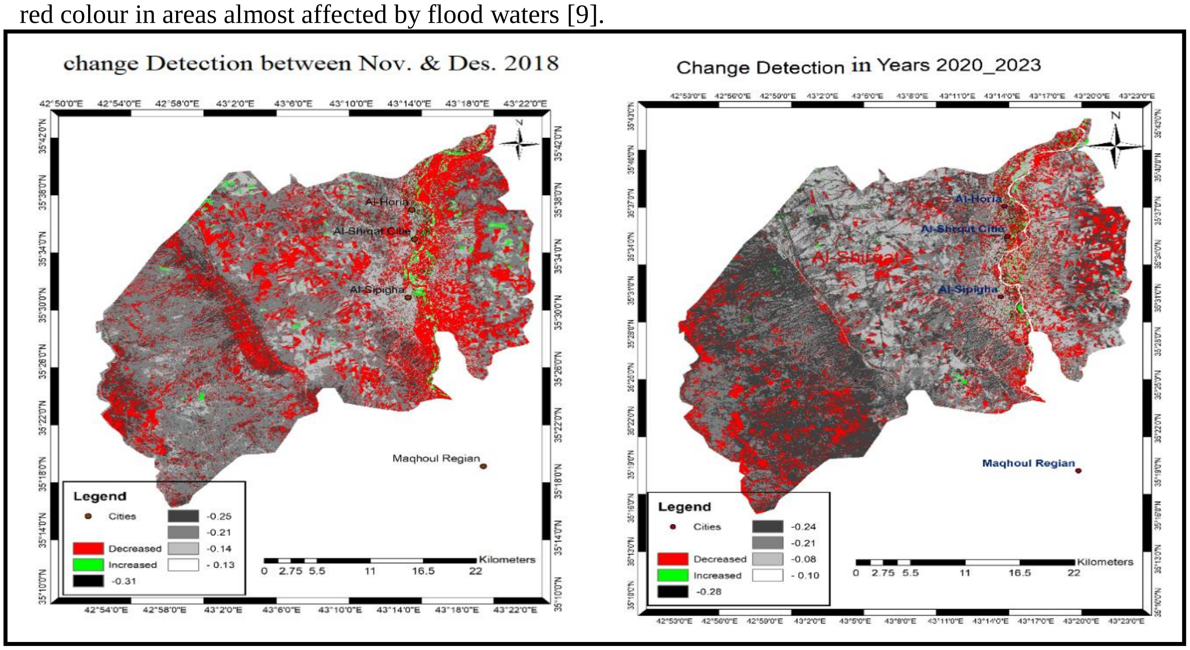

Fig. 7. The comparison result of Change Detection in different years

In this section, this study applied the change detection process, as shown in Figure 7, to calculate the area in square kilometers from the number of pixels [23], as the following Equations for Landsat 8;

$$\text{The images of } Landsat\ 8\ for\ the\ spatial\ resolution\ bands\ are\ 30m \times 30m \quad (3)$$

$$Area\ per\ pixel = 30 \times 30 = 900\ m^2 \quad (4)$$

$$convert\ to\ square\ kilometre, 1\ km^2 = 1{,}000{,}000\ m^2 \quad (5)$$

$$Area\ (km^2) = pixel\ count \times 0.0009 \quad (6)$$

Therefore, this equation for converting from pixels to area was applied in Table III and Table IV to represent the results of change detection for this study area, with the comparison flow chart in Figures 8a and Figures 8b.

TABLE III. CHANGE DETECTION BETWEEN NOV. & DES. 2018.

Category	Pixel count	Area (Km²)
Decreased	376,065	338.46
Some Decrease	700,753	630.68
Some Increase	376,533	338.88
Increased	18,561	16.70

TABLE IV. CHANGE DETECTION BETWEEN YEARS 2020 -2023

Category	Pixel count	Area (Km²)
Decreased	228,642	205.78
Some Decrease	1,001,175	901.06
Some Increase	231,689	208.52
Increased	10,405	9.36

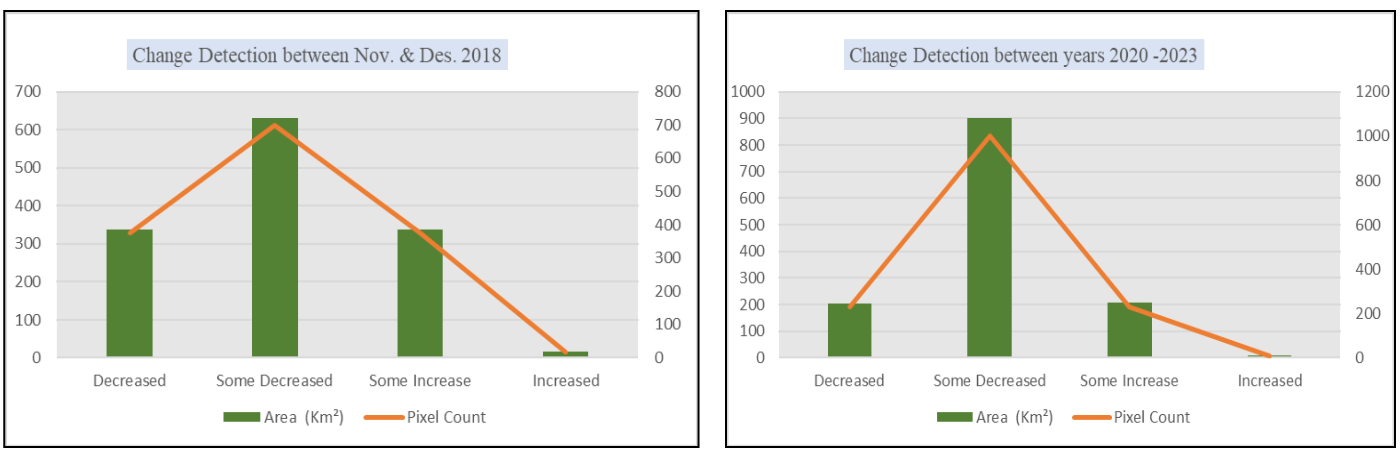

(a) (b)

Fig. 8. Land Change Monitoring: Comparative Analysis

The results of this application are unclear or unspecific for areas that experience floodwater dispersion during the chosen period, because the study area is located at the base of the mountains within the semi-mountainous region, where longitudinal, narrow, asymmetric convex folds characterise the Makhoul mountains. It will lead to faster water flow and less water retention in this area.

V. APPLICATION AND ANALYSIS MODEL BUILDER

A. Topography of the Study Area:

The topography of Al-Shirqat region was measured by using Geographic Information Systems (GIS) through a program ArcGIS v.10.2 to measure the highest and lowest points in the topography of the study area from the digital elevation model (DEM) from radar images that shows the terrain height on the surface of the earth, which is a source for numbering topographic maps and contour lines for this region [3]. To build a contour map of the study area by applying geology, geomorphology and hydrology to the study area to show the height of the terrain above ground level.

The topography is an essential factor for hydrological models to simulate flooding and runoff. One of the most obvious factors controlling stream flow is the gradient, or slope, of the river channel, as shown in Figure 9, which presents a demographic map and contours for the study area. The region's topography contributes to the risk of flooding in the lands adjacent to the river and at the base of the semi-mountainous Makhoul Mountains [11].

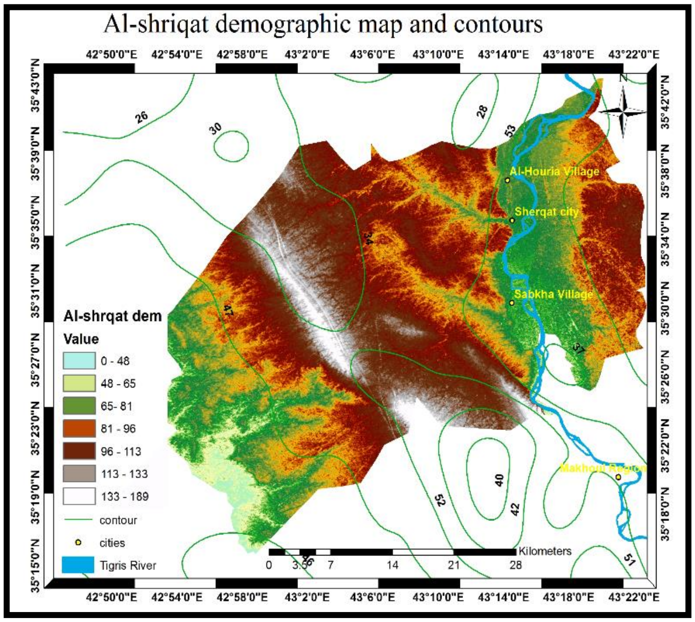

Fig. 9. Demography map and contours for the study area

B. Operation Flow Chart Model in ArcGIS:

Model Builder in ArcGIS, a visual software tool for building geo-processing workflows, automatically processes and documents spatial analysis and data management steps [17]. It is one of the hydrologic tools used to simulate surface water flow, based on DEM data [20]. Geo-processing models can be created and modified in the Model Builder to represent a graph that brings together a series of analysis and geo-processing tools in ArcGIS, using the output of one process as input to another [6]. Figure 10 below illustrates water flow and areas in the Al-Shirqat region.

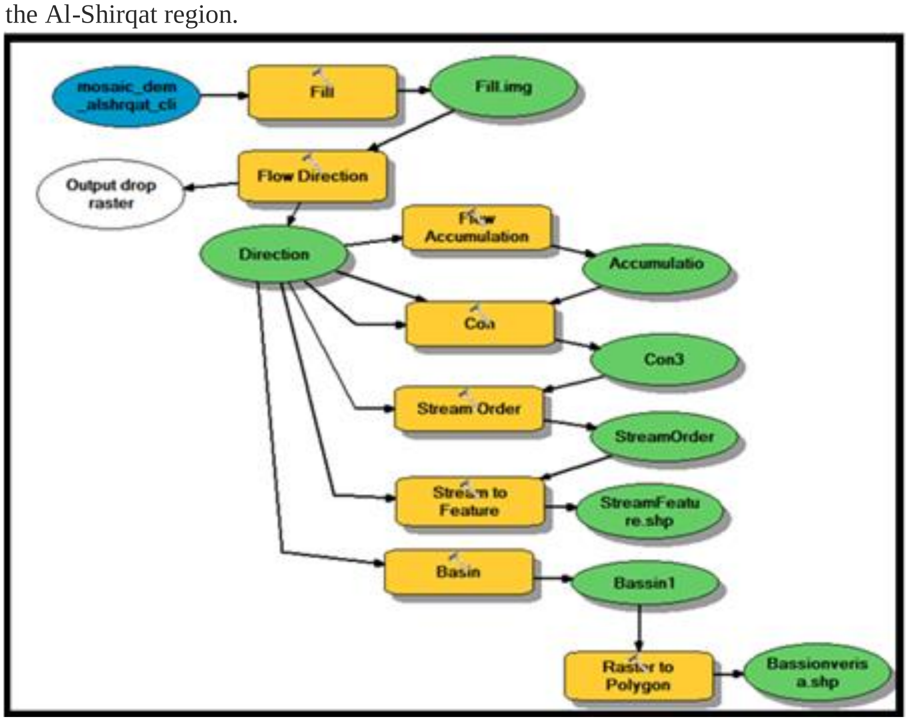

Fig. 10. Process flow chart by model builder in ArcGIS

C. Slopes and Flow Levels

The slope represents the rate of change in elevation for each digital elevation model (DEM) cell. It's the first derivative of a DEM, which is considered among the various techniques available for slope estimation [21]. In contrast, the flow level is a position that provides methods for describing the physical components of a hydrologic surface to measure runoff volume and for integrating physical soil data [22]. Therefore, the flood inundation is the accumulated level index that overflows the banks of the main river. It indicates the depth resulting from a river overflowing its banks, or is defined as the accumulated level index [18]. Flood inundation mapping aims to build scenarios for mitigation and response planning. The actual calculation of flood inundation required a data set comprising a DEM, flow direction, and river network. The Relative DEM simplifies mapping the inundation depth onto the landscape [9], as shown in Figure 11.

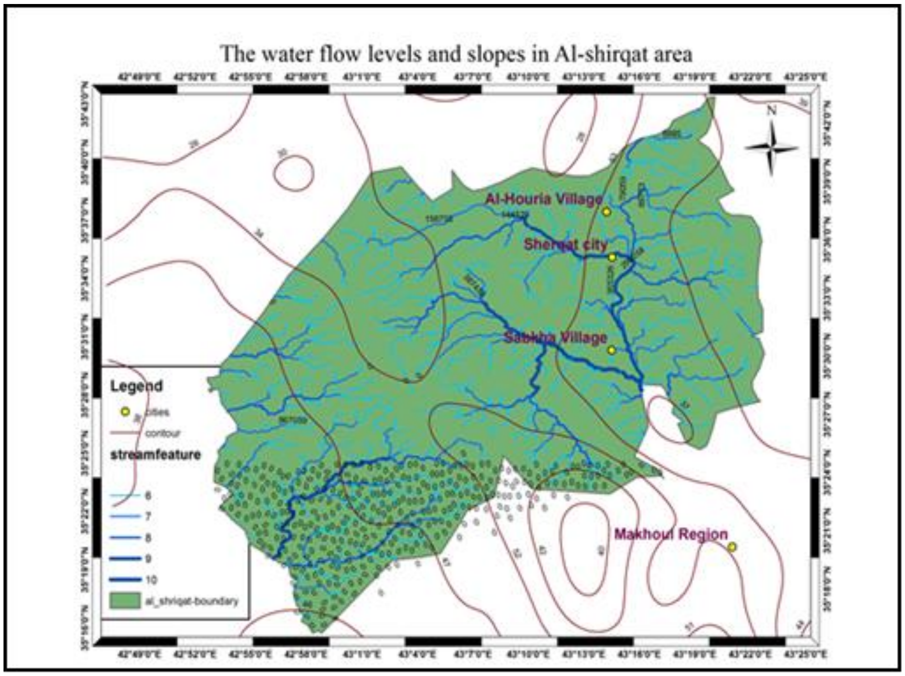

Fig. 11. The water flow levels and slopes for the study area

Furthermore, the flood level in the study area can also be represented by using. ARCSCENE v. 10.4.1, depending on the model builder [19] in ARCGIS v. 10.4.1, and Figure 12 explained the six stages of flooding extension levels in the study area.

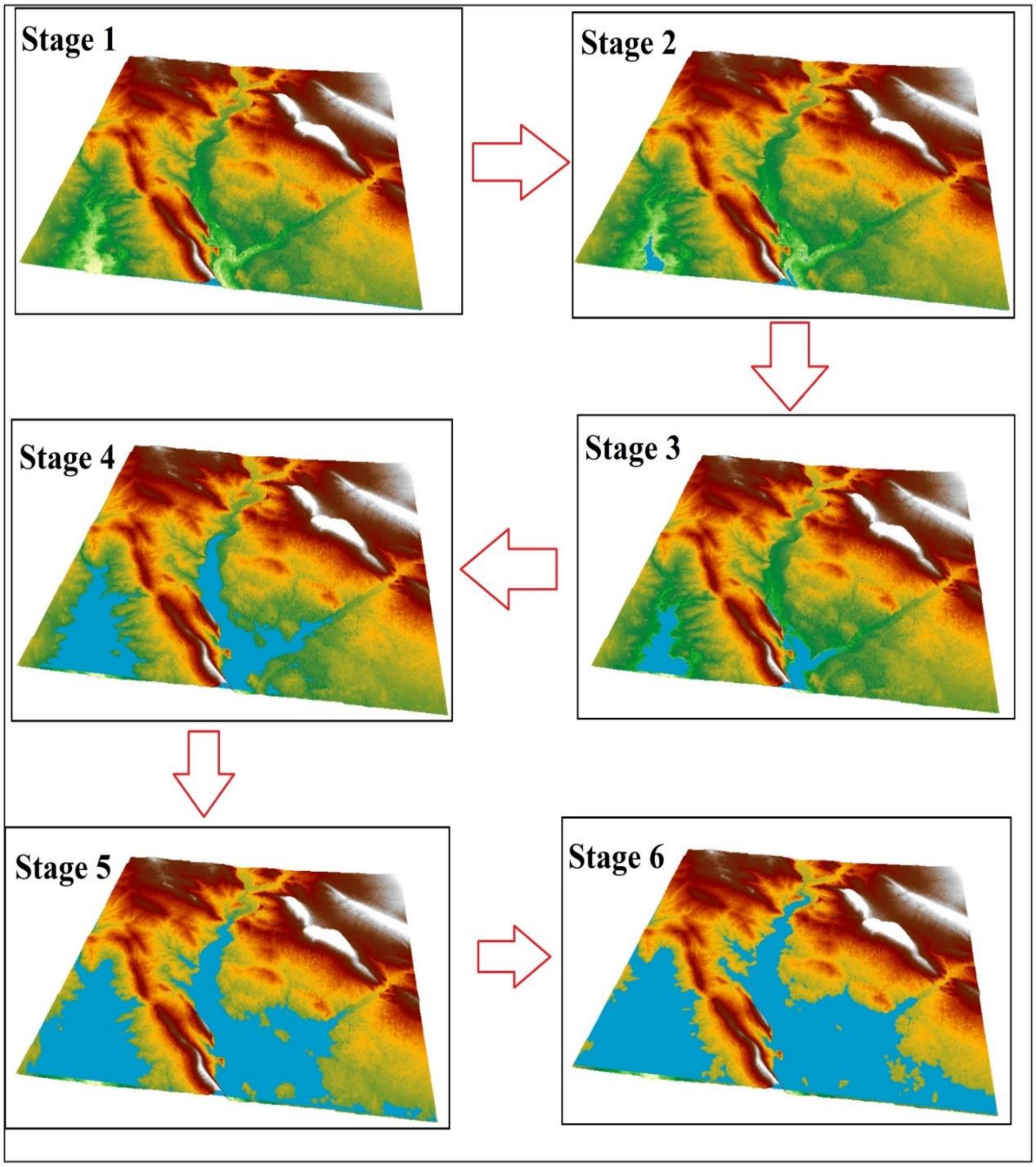

Fig. 12. Stages of flood extent levels.

VI. RESULT & CONCLUSION

The findings of this study, which involve a comparative analysis of historical flood inundation events and dry period conditions, can be integrated with supplementary geographic data—such as administrative boundaries, transportation networks, and land use/land cover (LULC) information—to assess the susceptibility of areas along streams and rivers to flooding. Furthermore, these findings provide a valuable basis for informed planning and the development of effective mitigation strategies to reduce the adverse impacts of flood inundation. Accordingly, the flooding of the Al-Shirqat region, which occurred over a short period, can be attributed to the following factors:

1) The volume of water inflow to the Tigris River from both internal and external sources exceeded normal levels due to intense rainfall during the wet hydrological year (2018–2019), particularly over a short period in November 2018. During the interval from 11 November to 12 December (approximately one month), in addition to the elevated water levels originating from the upper reaches of the Tigris River, further contributed to significant hydrological stress in the region, compared with the dry period observed between 2020 and 2023.
2) The topography of the study area, which is located at the foothills of mountainous terrain within a semi-mountainous region, presents challenges for the detection and analysis of geological changes using mathematical modelling approaches like the

NDWI) An equation used in this research to measure the spectral reflectivity of water shapes that remain in a specific place for a long time.

3) The application of modelling approaches, particularly those based on water reflectance derived from satellite imagery, represents an effective method for estimating floodwater levels in the Al-Shirqat region. This approach is especially suitable given the rapid onset of flooding from intense rainfall, the sharp rise in the Tigris River's water level over a short period, and the subsequent rapid recession of floodwaters from affected areas. For instance, the village of Al-Houriya experienced more severe impacts from the flood event than other locations, such as the city of Al-Shirqat and the village of Al-Sabkha, despite their locations along the same river reach.
4) The modelling builder methods can convert satellite images from raster to vector format with high accuracy and in a short time. It can simplify several processing steps, enabling the algorithms for the DEM surface to merge with visible satellite images. This allows quick identification of temporary, non-continuous flood spots within the research study area.
5) Finally, using a modelling approach in ArcGIS with the water indices will provide information on slope and water flow from topographic data of the research region, which will be useful. These outputs help geomatics researchers and dam engineers make smart decisions on where to build a dam in this area.

REFERENCES

[1] P. A. Brivio, R. Colombo, M. Maggi, and R. Tomasoni, 'Integration of remote sensing data and GIS for accurate mapping of flooded areas', Int. J. Remote Sens., vol. 23, no. 3, pp. 429–441, Jan. 2002, doi: 10.1080/01431160010014729.

[2] M. Safaripour, M. Monavari, M. Zare, Z. Abedi, and A. Gharagozlou, 'Flood Risk Assessment Using GIS (Case Study: Golestan Province, Iran)', Polish J. Environ. Stud., vol. 21, no. 6, pp. 1817–1824, 2012, [Online]. Available: https://api.semanticscholar.org/CorpusID:15377812

[3] [3] R. Mukhaiyar and U. Mukhaiyar, 'Attributes Classification for Elaborating the Information of Digital and Imaging Mapping', JOIV Int. J. Informatics Vis., vol. 8, no. 3–2, p. 1545, Nov. 2024, doi: 10.62527/joiv.8.3-2.2353.

[4] Purwadi, N. A. Abu, O. Mohd, B. A. Kusuma, and A. Ahmad, 'A Slab Multi-Fold Classification Technique on A Mixed Pixel Hyperspectral Image', JOIV Int. J. Informatics Vis., vol. 9, no. 5, p. 2192, Sep. 2025, doi: 10.62527/joiv.9.5.3432.

[5] P. Razi, A. Putri, J. T. Sri Sumantyo, and - Akmam, 'Vulnerability Liquefaction Mapping in Padang City Based on Cloud Computing Using Optical Satellite Imagery Data', JOIV Int. J. Informatics Vis., vol. 8, no. 3–2, p. 1932, Nov. 2024, doi: 10.62527/joiv.8.3-2.3480.

[6] A. H. Musarhad, M. J. Farhan, and A. A. Khalaf, 'Evaluation of the Fertility Status of some Soil Series of the North Tikrit Agricultural Project using Geospatial Technologies', IOP Conf. Ser. Earth Environ. Sci., vol. 1158, no. 2, p. 022032, Apr. 2023, doi: 10.1088/1755-1315/1158/2/022032.

[7] R. J. Radke, S. Andra, O. Al-Kofahi, and B. Roysam, 'Image change detection algorithms: a systematic survey', IEEE Trans. Image Process., vol. 14, no. 3, pp. 294–307, Mar. 2005, doi: 10.1109/TIP.2004.838698.

[8] Q. Zhao, S. Liu, L. Deng, S. Dong, Z. Yang, and Q. Liu, 'Determining the influencing distance of dam construction and reservoir impoundment on land use: A case study of Manwan Dam, Lancang River', Ecol. Eng., vol. 53, pp. 235–242, Apr. 2013, doi: 10.1016/j.ecoleng.2012.12.050.

[9] E. R. Myers, D. M. Browning, L. M. Burkett, D. K. James, and B. T. Bestelmeyer, 'Novel Use of Image Time Series to Distinguish Dryland Vegetation Responses to Wet and Dry Years', J. Remote Sens., vol. 4, Jan. 2024, doi: 10.34133/remotesensing.0190.

[10] M. A. Salman, M. S. S. Nomaan, S. Sayed, A. Saha, and M. R. Rafiq, 'land use and land cover change detection by using remote sensing and gis technology in barishal district, bangladesh', Earth Sci. Malaysia, vol. 5, no. 1, pp. 33–40, Dec. 2020, doi: 10.26480/esmy.01.2021.33.40.

[11] S. N. Hussein, B. K. Nile, and H. M. Zwain, 'Evaluation and determination of flood areas using SWMM and the creation of a mathematical model using dimensional analysis: A case study of the city of Najaf', in the 6th international conference on energy, environment, epidemiology and information system (icenis) (ICENIS) 2021: Topic of Energy, Environment, Epidemiology, and Information System, 2023, p. 020023. doi: 10.1063/5.0131176.

[12] Nehad Hameed Al-salmany and Taghreed Abdalhameed Naji, 'The Effect of Satellite Image Fusion on the Classification Process by Using Multiple Sensors', Iraqi Natl. J. Earth Sci., vol. 25, no. 1, pp. 103–122, Jan. 2025, doi: 10.33899/earth.2024.143380.1145.

[13] N. Gorelick, M. Hancher, M. Dixon, S. Ilyushchenko, D. Thau, and R. Moore, 'Google Earth Engine: Planetary-scale geospatial analysis for everyone', Remote Sens. Environ., vol. 202, pp. 18–27, Dec. 2017, doi: 10.1016/j.rse.2017.06.031.

[14] S. M. Shravan Kumar, M. Pandey, and A. K. Shukla, 'Spatio-temporal analysis of riverbank changes using remote sensing and geographic information system', Phys. Chem. Earth, Parts A/B/C, vol. 136, p. 103692, Dec. 2024, doi: 10.1016/j.pce.2024.103692.

[15] M. C. Velandia-García, D. Luna-Naranjo, and J. D. López, 'Ecological Land Cover Classification Through LDA on Combination Spectral Features from Multi-source Satellite Imagery', in Workshop on Engineering Applications, 2026, pp. 292–303. doi: 10.1007/978-3-032-08206-0_25.

[16] S. K. Srivastava, R. D. Gupta, and others, 'Monitoring of changes in land use/land cover using multi-sensor satellite data', GIS Dev. Map India, 2003.

[17] L. Thi Minh Phuong and B. Hai Phong, 'A New Approach for The Automation of Spatial Data Updates Using ArcGIS ModelBuilder for Provincial Planning in The Region of Nghe An, Vietnam', Int. J. Sustain. Constr. Eng. Technol., vol. 16, no. 2, Sep. 2025, doi: 10.30880/ijscet.2025.16.02.011.

[18] H. Desalegn and A. Mulu, 'Mapping flood inundation areas using GIS and HEC-RAS model at Fetam River, Upper Abbay Basin, Ethiopia', Sci. African, vol. 12, p. e00834, Jul. 2021, doi: 10.1016/j.sciaf.2021.e00834.

[19] F. Pedrero, J. J. Alarcón, M. Abellán, and P. Perez-Cutillas, 'Optimisation of the use of reclaimed water through groundwater recharge, using a Geographic Information System', Desalin. Water Treat., vol. 57, no. 11, pp. 4864–4877, Mar. 2016, doi: 10.1080/19443994.2014.1003979.

[20] A. Ali, 'Watershed Delineation from DEM by Model Builder in ArcGIS' Civil Engineering Journal Vol. 9, No. 11, November, 2023, doi: 10.28991/cej-2023-09-11-011.

[21] C. Nunez, J. Parrot, C. Siebe and L. Selem 'Semiautomated classification of units in volcanic terrain based on three morphometric attributes derived from a digital elevation model (DEM)' Earth Surface Processes and Landforms Vol. 5, Issue 6, June 2026, doi: epdf/10.1002/esp.70299.

[22] S. Ricard, et al. 'Assessing the Impacts of Soil Conservation Practices on Surface Runoff and Water Quality Using an Agricultural Experimental Setup, Generalised Additive Mixed Models, and Hydrologic Modelling' Hydrological Processes, Vol. 39, Issue 4, Aprail 2025, doi.org/ 10.1002/hyp.70126.

[23] J. Chen et al. 'The Performance of Landsat-8 and Landsat-9 Data for Water Body Extraction Based on Various Water Indices: A Comparative Analysis' Remote Sensing Journals, Vol. 16 Issue 11, May 2024, doi.org/ 10.3390/rs16111984.